

# Manifestation of a topological gapless phase in a two-dimensional chiral symmetric system through Loschmidt echo

K. L. Zhang and Z. Song\*

*School of Physics, Nankai University, Tianjin 300071, China*

Unlike the edge state of a topological insulator where its energy level lives in the bulk energy gap, the edge state of a topological semimetal hides in the bulk spectrum and is difficult to be identified by the energy. We investigate the sensitivity of bulk and edge states of the gapless phase for a topological semimetal to the disordered perturbation via a concrete two-dimensional chiral symmetric lattice model. The topological gapless phase is characterized by two opposite vortices in the momentum space and nonzero winding numbers, which correspond to the edge flatband when the open boundary condition is applied. For this system, numerical results reveal that a distinguishing feature is that the robustness of the edge states against weak disorder and the flatband edge modes remain locked at zero energy in the presence of weak chiral-symmetry-preserving disorder. We employ the Loschmidt echo (LE) for both bulk and edge states to study the dynamic effect of disordered perturbation. We show that, for an initial bulk state, the LE decays exponentially, whereas it converges to a constant for an initial edge state in the presence of weak disorder. Furthermore, the convergent LE can be utilized to identify the positions of vortices as well as the phase diagram. We discuss the realization of such dynamic investigations in a topological photonic system.

## I. INTRODUCTION

Topological state of matter<sup>1–4</sup> have become the focus of intense research in many branches of physics and provides a fertile ground for demonstrating the concepts in high-energy physics, including Majorana<sup>5–10</sup>, Dirac<sup>11–17</sup> and Weyl fermions<sup>18–26</sup>. These concepts relate to topological gapless phases and corresponding edge modes, not only exhibiting new physical phenomena with potential technological applications, but also deepening our understanding on state of matters. System in the topological gapless phase exhibits band structures with band-touching points in the momentum space, where these kinds of nodal points appear as topological defects of Bloch vector field. On the other hand, a gapped phase can be topologically non-trivial, commonly referred to as topological insulators and superconductors. Such phase is associated at least with two isolated bulk energy bands, where the band structure of each is characterized by non-trivial topological index. A particularly important concept is the bulk-boundary correspondence, which links the nontrivial topological invariant in the bulk to the localized edge modes. In general, edge states are the eigenstates of Hamiltonian that are exponentially localized at the boundary of the system. A gapped topological phase is always associated with an bulk energy gap, while a topological gapless phase, commonly referred to as topological semimetals and nodal superconductors, can exhibit topological protected Fermi points or nodal points (We refer to the bulk energy gap as the energy gap of the system with translational symmetry and without disorder throughout this paper). Accordingly, unlike the edge state of a topological insulator, where its energy level lives in the bulk energy gap, the edge state of a topological gapless phase hides in the bulk spectrum, and is hard to be identified by the energy. These edge states can form partial flat band in a ribbon geometry<sup>27–29</sup>,

which also exhibit robustness against disorder<sup>30</sup>. Recently, it has been pointed that Majorana zero modes are not only attributed to topological superconductors. A two-dimensional (2D) topologically trivial superconductors without chiral edge modes can host robust Majorana zero modes in topological defects<sup>31–33</sup>. In experimental aspect, photonic systems provide a convenient and versatile platform to design various topological lattice models and study different topological states<sup>34,35</sup>.

In this paper, we investigate the sensitivity of bulk and edge states of gapless phase for topological semimetal to the disordered perturbation via a concrete two-dimensional chiral symmetric lattice model. We employ the Loschmidt echo (LE) for both bulk and edge states to study the dynamic effect of disordered perturbation. The LE is a measure of the revival occurring when an imperfect time-reversal procedure is applied to a complex quantum system. It allows to quantify the sensitivity of quantum evolution to perturbations. This work aims to shed light on the nature of topological edge modes associated with gapless phase for topological semimetal with chiral symmetry, rather than gapped topological materials. We show that for a initial bulk state LE decays exponentially, while converges to a constant for an initial edge state in the presence of weak chiral-symmetry-preserving disorder. Our results provide a dynamic way to identify topological edge states arising from topological gapless phase in 2D chiral symmetric system. The reason is that unlike the edge states in topological insulator, here the edge flat band hides in a continuous spectrum. There is no bulk energy gap to protect the channel of the edge states. Thanks to the photonic system, where the Pauli exclusion not obeyed, a single-particle state can be amplified by the large population of photons. The phase diagram can be detected by using edge-state photon dynamics.

This paper is organized as follows. In Sec. II, we present the introduction of Loschmidt echo and the idea

about apply it to the bulk and edge states in gapless systems. In Sec. III, we introduce a square lattice without disorder to illustrate our method. Section IV focus on the dynamics of the system in the presence of disorder, and demonstrates the dynamics method of detect edge modes. Finally, our conclusion and discussion are given in Sec. V.

## II. EDGE STATES AND LOSCHMIDT ECHO

Anderson localization is a basic condensed matter physics phenomenon, which describes the absence of diffusion of waves in a disordered medium<sup>36</sup>. It turns out that particle localization is possible in a lattice potential, provided that the strength of disorder in the lattice is sufficiently large. The confinement of waves in a disordered medium has been observed for electromagnetic<sup>37,38</sup> and acoustic<sup>39</sup> waves in disordered dielectric structures, and for electron waves in condensed matter. On the other hand, to capture the effect of disorder on the dynamics, one can employ a concept of LE or fidelity. LE is a measure of reversibility and sensitivity to perturbations of quantum evolutions. An initial quantum state  $|\psi(0)\rangle$  evolves during a time  $T$  under a Hamiltonian  $H_0$  reaching the state  $|\psi(t)\rangle$ . Aiming to recover the initial state  $|\psi(0)\rangle$  a new Hamiltonian  $H$  is applied between  $T$  and  $2T$ . Quantity  $|\langle\psi(0)|e^{-iHt}e^{-iH_0t}|\psi(0)\rangle|^2$  is induced to measure the fidelity of this recovery. Perfect recover of  $|\psi(0)\rangle$  would be achieved by choosing  $H = -H_0$ . In the context of the present work, the LE is defined as

$$M(t) = |\langle\psi(0)|e^{iH_D t}e^{-iH_0 t}|\psi(0)\rangle|^2, \quad (1)$$

where  $|\psi(0)\rangle$  is the state of the system at time  $t = 0$ ,  $H_0$  is the Hamiltonian of uniform system,  $H_D$  is the Hamiltonian  $H_0$  under disordered perturbation. For certain topological non-trivial systems, edge states are robust under a weak symmetry-preserving disorder, still being localized state<sup>34,40,41</sup>. Particularly, we numerically observe that the corresponding eigen energy is locked at zero, as it is shown through a concrete model in Sec. IV. Therefore, considering such a topological system, it is expected that (i) when an initial quantum state  $|\psi(0)\rangle$  is a local state at bulk,  $M(t)$  could decay to zero due to the fact that  $e^{-iH_0 t}|\psi(0)\rangle$  and  $e^{-iH_D t}|\psi(0)\rangle$  diffuse in 2D space in different ways, (ii) when  $|\psi(0)\rangle$  is an edge state of  $H_0$ ,  $M(t)$  could be the constant 1.

Here we consider the LE for a local state  $|\psi(0)\rangle$  at the edges. We note that  $|\psi(0)\rangle$  is almost be written as the superposition of the flat band edge modes of  $H_0$  or  $H_D$ , respectively, which result in

$$H_0|\psi(0)\rangle \approx 0, H_D|\psi(0)\rangle \approx 0, \quad (2)$$

for weak disordered perturbation  $H_D - H_0 \ll H_0$ . Then we always have

$$\begin{aligned} M(t) &= |\langle\psi(0)|e^{iH_D t}e^{-iH_0 t}|\psi(0)\rangle|^2 \\ &\approx |\langle\psi(0)|\psi(0)\rangle|^2 = 1. \end{aligned} \quad (3)$$

In the following, we will demonstrate this analysis through a concrete example.

## III. MODEL WITHOUT DISORDER

We focus on a concrete 2D chiral symmetric model to demonstrate the main idea. In the previous works<sup>42,43</sup> we have demonstrated that a topologically trivial superconductor emerges as a topological gapless state, which support Majorana flat band edge modes. The quantum state is characterized by two band-degeneracy points with opposite chirality. In the present work, we directly consider a tight-binding model with the same structure as the Majorana lattice. In the following, (i) we present the Hamiltonian and the phase diagram for the topological gapless phase; (ii) we investigate the topological edge states with nonzero winding numbers.

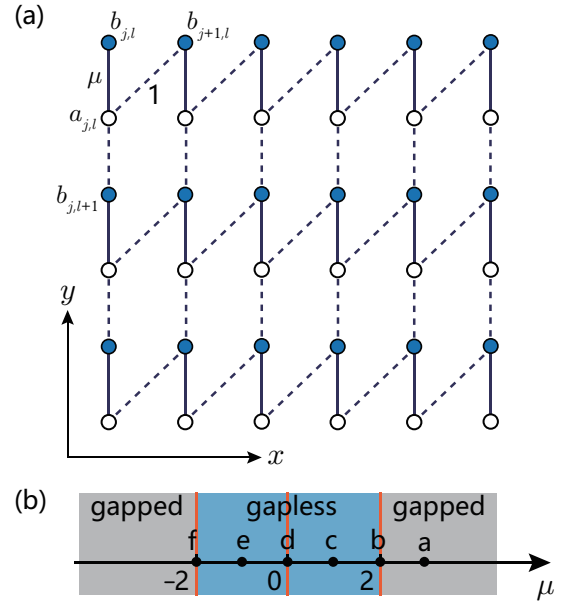


FIG. 1. (a) Schematic illustration of the 2D tight-binding model with Hamiltonian Eq. (4), which is essentially a bipartite  $M \times N$  honeycomb lattice. The solid lines and dashed lines represent hopping terms with strengths  $\mu$  and 1, respectively. (b) Phase diagram of the lattice system with parameter  $\mu$ . The orange lines indicate the phase boundary, which separate the topologically trivial gapped phases (gray) and topological gapless phases (blue). The system with parameter at the boundary (orange lines) is topologically trivial gapless phase. Points (a-f) represent the systems in each phases, which are extensively investigated in Fig. 3.

### A. Model and topological gapless phase

We consider a tight-binding model on a bipartite  $M \times N$  lattice with the Hamiltonian

$$H = \sum_{\mathbf{r}} (\mu a_{\mathbf{r}}^\dagger b_{\mathbf{r}} + a_{\mathbf{r}}^\dagger b_{\mathbf{r}+\hat{x}} + a_{\mathbf{r}}^\dagger b_{\mathbf{r}+\hat{y}}) + \text{h.c.}, \quad (4)$$

where  $\mathbf{r} = (j, l)$  is the coordinates of lattice sites and  $a_{\mathbf{r}}$  and  $b_{\mathbf{r}}$  are the fermion or boson annihilation operators at site  $\mathbf{r}$  in sublattice of A and B, respectively. Vectors  $\hat{x}$ ,  $\hat{y}$ , are the unitary lattice vectors in the  $x$  and  $y$  directions. The hopping between neighboring sites is described by the hopping amplitudes  $\mu$  and 1. The schematic diagram for the honeycomb lattice is shown in Fig. 1(a). This simple model can be regarded as a strained graphene lattice<sup>44–48</sup> which is uniaxially strained along the  $y$  direction.

We introduce the Fourier transformations

$$(a_{\mathbf{k}}, b_{\mathbf{k}}) = \frac{1}{\sqrt{MN}} \sum_{\mathbf{r}} (a_{\mathbf{r}}, b_{\mathbf{r}}) e^{-i\mathbf{k} \cdot \mathbf{r}}. \quad (5)$$

Then the Hamiltonian with periodic boundary conditions on both directions can be block diagonalized as

$$H = \sum_{\mathbf{k}} \begin{pmatrix} a_{\mathbf{k}}^\dagger & b_{\mathbf{k}}^\dagger \end{pmatrix} h(\mathbf{k}) \begin{pmatrix} a_{\mathbf{k}} \\ b_{\mathbf{k}} \end{pmatrix}, \quad (6)$$

with the core matrix

$$h(\mathbf{k}) = \begin{pmatrix} 0 & g(\mathbf{k}) \\ g^*(\mathbf{k}) & 0 \end{pmatrix}, \quad (7)$$

and  $g(\mathbf{k}) = \mu + (e^{ik_x} + e^{ik_y})$ . We note that the system respects time reversal, chiral, and particle-hole symmetry, i.e., for the Bloch Hamiltonian  $h(\mathbf{k})$ , we have  $\mathcal{T}h(\mathbf{k})\mathcal{T}^{-1} = h(-\mathbf{k})$ ,  $\mathcal{S}h(\mathbf{k})\mathcal{S}^{-1} = -h(\mathbf{k})$ , and  $\mathcal{C}h(\mathbf{k})\mathcal{C}^{-1} = -h(-\mathbf{k})$ , with  $\mathcal{T} = \mathcal{K}$  is the complex conjugation operator and  $\mathcal{S} = \sigma_z$ ,  $\mathcal{C} = \sigma_z \mathcal{K}$ . The core matrix can be written as

$$h(\mathbf{k}) = \mathbf{B}(\mathbf{k}) \cdot \boldsymbol{\sigma}, \quad (8)$$

where the components of the Bloch vector  $\mathbf{B}(\mathbf{k}) = (B_x, B_y, B_z)$  are

$$\begin{cases} B_x = \mu + (\cos k_x + \cos k_y) \\ B_y = -(\sin k_x + \sin k_y) \\ B_z = 0 \end{cases}, \quad (9)$$

and  $\boldsymbol{\sigma} = (\sigma_x, \sigma_y, \sigma_z)$  are the Pauli matrices. The spectrum is

$$E_{\mathbf{k}}^\pm = \pm \sqrt{(\mu + \cos k_x + \cos k_y)^2 + (\sin k_x + \sin k_y)^2}. \quad (10)$$

We focus on the gapless phase arising from the band degenerate points of the spectrum. The band degenerate point  $\mathbf{k}_0 = (k_{0x}, k_{0y})$  fulfill the equations

$$\begin{cases} \sin k_{0x} + \sin k_{0y} = 0 \\ \mu + \cos k_{0x} + \cos k_{0y} = 0 \end{cases}. \quad (11)$$

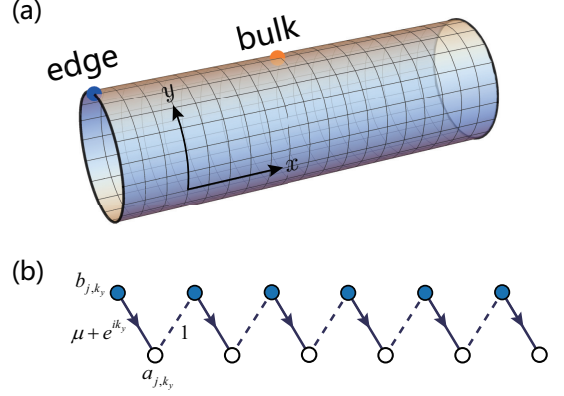


FIG. 2. (a) Schematic illustration of the geometry of the system with cylindrical boundary condition. The locations of initial local states at edge (blue dot) and bulk (orange dot) of the 2D lattice system are indicated. (b) Schematic illustration of the modified SSH chain  $H_k$  represented in Eq. (18). The arrows and dashed lines represent complex and real hopping terms,  $(\mu + e^{ik})$  and 1, respectively. The edge modes of a set of modified SSH chains form the flat band edge modes as bound states located at two edges of the cylinder when the system is in the blue region of the phase diagram in Fig. 1(b).

As shown in Fig. 3(a1)-(f1), there have three types of bands touching configurations: single point, double points, and lines in the  $k_x$ - $k_y$  plane, determined by the parameter  $\mu$ . We are interested in the non-trivial case (double points) with nonzero  $\mu$ . Then from Eq. (11), we have

$$k_{0x} = -k_{0y} = \pm \arccos(-\frac{\mu}{2}), \quad (12)$$

in the condition of  $|\mu| \leq 2$ . It indicates that there are two degenerate points for  $\mu \neq 0$  and  $|\mu| \neq 2$ . When  $\mu$  vary, the two points move along the line:  $k_{0x} = -k_{0y}$ , and merge at  $\mathbf{k}_0 = (\pm\pi, \mp\pi)$  or  $\mathbf{k}_0 = (0, 0)$  when  $\mu = 2$  or  $\mu = -2$ . In the case of  $\mu = 0$ , the degenerate points become two degenerate lines:  $k_{0y} = \pm\pi + k_{0x}$ . The phase diagram is shown in Fig. 1(b) and the bulk spectra for several typical cases are illustrated in Fig. 3(a1)-(f1).

The gapless phase of this model can be protected by a  $\mathbb{Z}$ -type invariant according to the classification topological semimetals<sup>3,49</sup>. For isolated band touching point, the topological nature of the band degeneracy can be considered as a vortex in the momentum space with integer winding numbers, which is equivalent to concept of the Berry flux<sup>50,51</sup>. The Berry flux is defined as the contour integral of the Berry connection in the momentum space<sup>50,52</sup>. A band degenerate point can be regarded as a topological defect and the topological index can be extracted from the expression of Bloch vector  $\mathbf{B}(\mathbf{k})$ . Actually, in the vicinity of the degenerate points, the Bloch vector can be expressed as the from

$$\begin{cases} B_x = -\sin k_{0x} (q_x - q_y) \\ B_y = -\cos k_{0x} (q_x + q_y) \\ B_z = 0 \end{cases}, \quad (13)$$

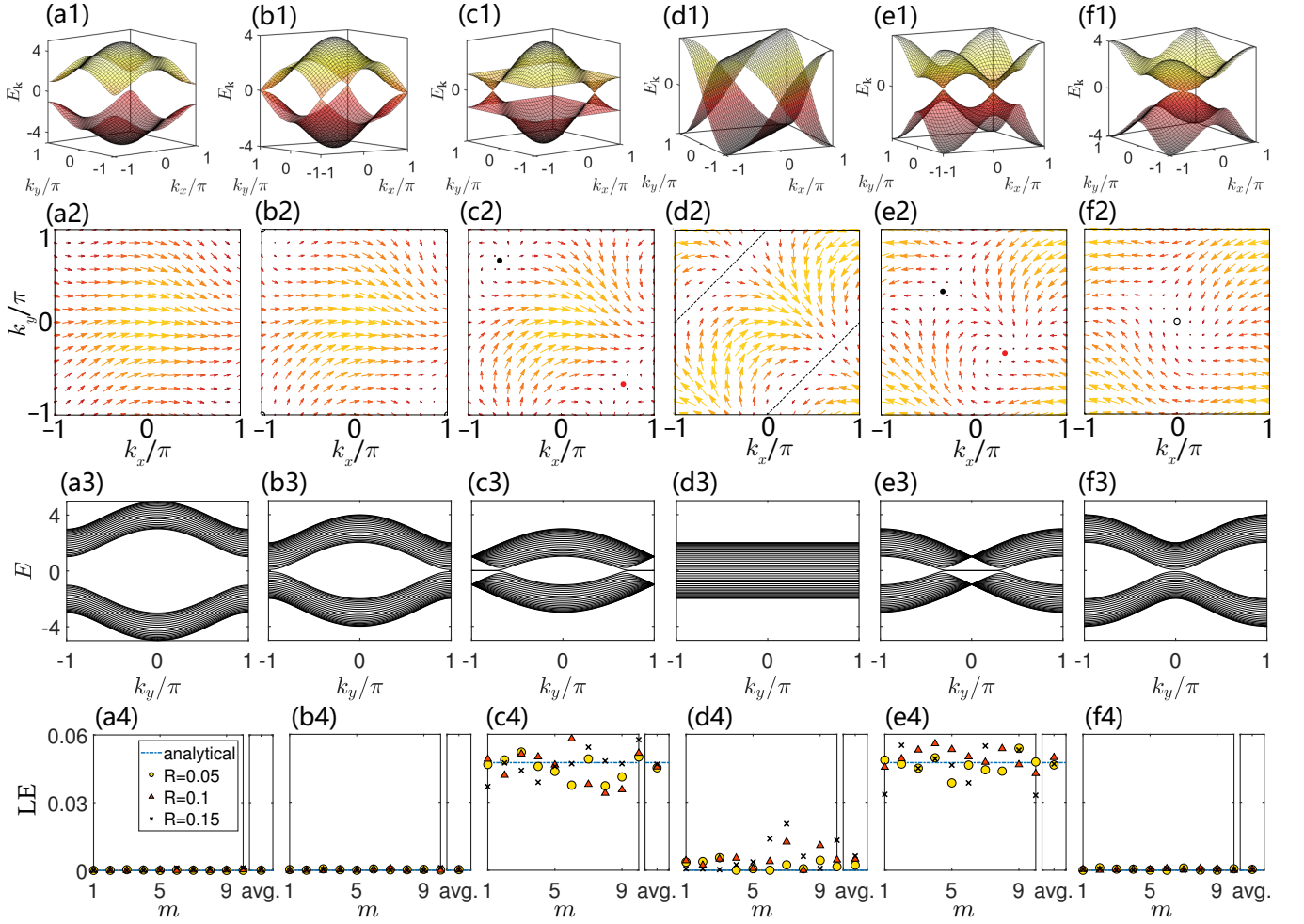


FIG. 3. Kaleidoscope of quantum phases. (a1)-(f1) Plots of energy spectra from Eq. (10) at six typical points (a-f) marked in the phase diagram in Fig. 1(b). There, the band structure exhibits a bulk gap in (a1); a single degeneracy point with parabolic dispersion in (b1) and (f1); two degeneracy points with linear dispersion in (c1) and (e1); and two degeneracy lines in (d1). (a2)-(f2) Plots of Bloch vector field defined in Eq. (9) in the momentum space for six cases corresponding to (a1)-(f1). There are two vortices in (c2) and (e2) with opposite winding numbers  $\pm 1$ . As  $\mu$  increases or decrease, two vortices get close and merge into a single point in (b2) or (f2), and disappears in (a2). (a3)-(f3) Plots of the spectra of a set of modified SSH chains (Eq. (17)) in open boundary condition with  $N = 40$  for six cases corresponding to (a1)-(f1). It indicates that the existence of pair of vortices links to a flat band of the square lattice. (a4)-(f4) Plots of LE obtained by numerical simulations from Eq. (1) at  $t = 3000J^{-1}$  and analytical expressions from Eq. (28), in which the initial state is taken as the site-state at the edge. Here  $J$  is the scale of the Hamiltonian and we take  $J = 1$ .  $R$  is the disorder strength and  $m$  denotes the measurement index. The average value of LEs are plotted in the right of each panel. The size of the system is  $M \times N = 80 \times 80$ .

where  $\mathbf{q} = \mathbf{k} - \mathbf{k}_0$  is the momentum in another frame and  $\mathbf{k}_0 = (k_{0x}, k_{0y})$  satisfy Eq. (12). Around these degenerate points, the core matrix  $h(\mathbf{k})$  can be linearized as

$$h(\mathbf{q}) = \sum_{i,j=1}^2 c_{ij} q_i \sigma_j, \quad (14)$$

which is equivalent to the Hamiltonian for 2D massless relativistic fermions. Here  $(q_1, q_2) = (q_x, q_y)$ ,  $(\sigma_1, \sigma_2) = (\sigma_x, \sigma_y)$  and  $c = \begin{pmatrix} -\sin k_{0x} & -\cos k_{0x} \\ \sin k_{0x} & -\cos k_{0x} \end{pmatrix}$ . The corresponding chirality for these particle is defined as

$$w = \text{sgn}[\det(c)] = \text{sgn}[\sin(2k_{0x})], \quad (15)$$

which leads to  $w = \pm 1$  for two degenerate points. The chiral relativistic fermions serve as 2D Dirac points. Two Dirac points located at two separated degenerate points have opposite chirality. We note that  $w = 0$  for  $\mu = 0$  and  $|\mu| = 2$ . When  $\mu = -2$  or  $\mu = 2$ , two Dirac points merge at  $(0, 0)$  or  $(\pm\pi, \mp\pi)$  and become a single degenerate point. The topology of the degenerate point becomes trivial, and a perturbation hence can open up the bulk energy gap. We illustrate the Bloch vector fields in  $k_x$ - $k_y$  plane for several typical cases in Fig. 3(a2)-(f2). As shown in figures, we find three types of topological configurations: pair of vortices with opposite chirality, single trivial vortex (or degeneracy lines), and no vor-

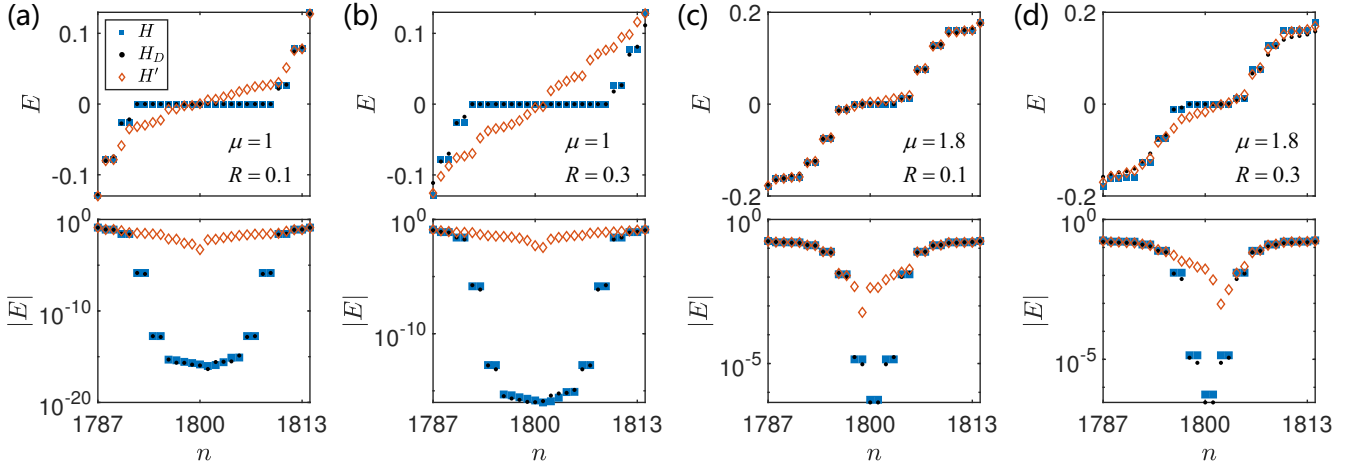


FIG. 4. Linear and log scale plots of eigenenergy around zero for  $H$ ,  $H_D$  and  $H'$  with cylindrical boundary condition.  $n$  denotes the sorting index. The parameters are  $\mu = 1$  for (a) and (b);  $\mu = 1.8$  for (c) and (d);  $R = 0.1$  for (a) and (c);  $R = 0.3$  for (b) and (d). It indicates that the number of zero modes is dependent on  $\mu$ , and the zero modes remain unchanged in the presence of chiral-symmetry-preserving disordered perturbation, while do not survive under the chiral-symmetry-breaking disordered perturbation. The results are obtained by numerical diagonalization for the system with  $M \times N = 60 \times 60$ .

tex, corresponding to topological gapless, trivial gapless and gapped phases, respectively. According to the bulk-boundary correspondence<sup>3,49</sup>, the nontrivial bulk topology would lead to the protected surface states and forming the flat band when the open boundary condition is applied, as we can see in the following.

### B. Flat band edge modes

Now we turn to study the feature of gapless phase of the square lattice. At first, we revisit the description of the present model with cylindrical boundary condition as shown in Fig. 2(a). Consider the Fourier transformations in  $y$  direction

$$(a_{j,k_y}, b_{j,k_y}) = \frac{1}{\sqrt{N}} \sum_{l=1}^N e^{-ik_y l} (a_{j,l}, b_{j,l}), \quad (16)$$

where the wave vector  $k_y = 2\pi n/N$ ,  $n = 1, 2, \dots, N$ . The Hamiltonian  $H$  can be rewritten as

$$H = \sum_{k_y} H_{k_y}, \quad (17)$$

with

$$H_{k_y} = \sum_{j=1}^N \delta_{k_y} a_{j,k_y}^\dagger b_{j,k_y} + \sum_{j=1}^{N-1} a_{j,k_y}^\dagger b_{j+1,k_y} + \text{h.c.}, \quad (18)$$

where  $\delta_{k_y} = (\mu + e^{ik_y})$ , and  $H_{k_y}$  obeys  $[H_{k_y}, H_{k'_y}] = 0$ , i.e.,  $H$  has been block diagonalized. We note that each  $H_{k_y}$  represents a modified Su-Schrieffer-Heeger (SSH) chain with hopping terms  $\delta_{k_y}$  and 1. The schematic diagram is shown in Fig. 2(b).

The flat band edge modes of 2D chiral symmetric Hamiltonian Eq. (4) with cylindrical boundary condition are originated from the zero energy edge states of the modified SSH in Eq. (18), which can be related to the winding number<sup>28,53–56</sup> or Zak phase<sup>57</sup>. The winding number for the bulk Hamiltonian of Eq. (18) is defined as<sup>56</sup>

$$\mathcal{W}(k_y) = \frac{1}{2\pi i} \int_{-\pi}^{\pi} dk_x \partial_{k_x} \ln g(\mathbf{k}), \quad (19)$$

where  $g(\mathbf{k})$  is an off-diagonal element of the core matrix  $h(\mathbf{k})$  of the 2D bulk Hamiltonian in Eq. (6). Direct derivation gives

$$\mathcal{W}(k_y) = \begin{cases} 1, & \mu(\mu + 2 \cos k_y) < 0 \\ 0, & \mu(\mu + 2 \cos k_y) > 0 \end{cases}. \quad (20)$$

The winding number is 1 for the parameters region  $\mu(\mu + 2 \cos k_y) < 0$ , in which the open chain in Eq. (18) is expected to exist 1 pairs of zero energy edge states<sup>55</sup>, localized at two ends of the chain, respectively. These zero energy edge states for all  $k_y$  in the above parameters region form the flat band edge modes for the 2D lattice with cylindrical geometry.

One can always get a diagonalized  $H_{k_y}$  through the diagonalization of the matrix of the corresponding single-particle SSH chain. Actually, it can be checked that  $H_{k_y}$  exists two zero modes in large  $N$  limit

$$\begin{cases} |\psi_R\rangle = \Omega \sum_{j=1}^N (-\delta_{k_y}^*)^{N-j} a_{j,k_y}^\dagger |\text{vac}\rangle \\ |\psi_L\rangle = \Omega \sum_{j=1}^N (-\delta_{k_y})^{j-1} b_{j,k_y}^\dagger |\text{vac}\rangle \end{cases}, \quad (21)$$

where  $\Omega = \sqrt{1 - |\delta_{k_y}|^2}$  is normalization constant, and  $|\delta_{k_y}| < 1$ , representing edge modes localizing at the



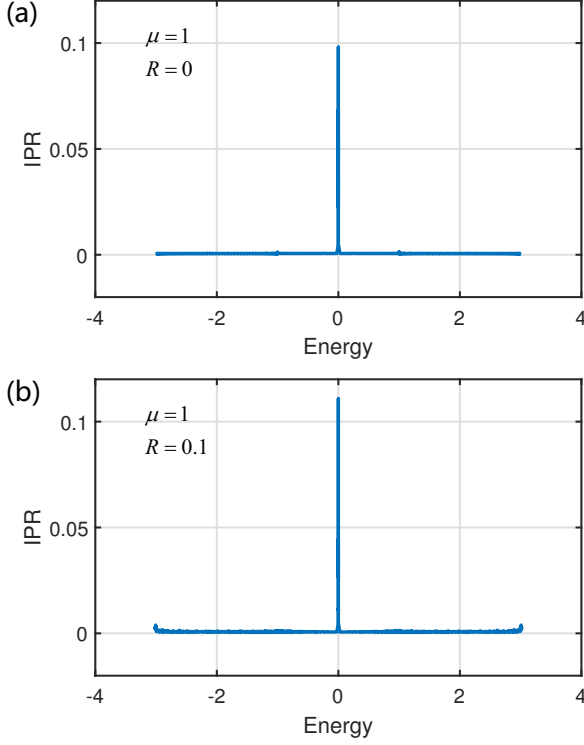


FIG. 5. Numerical results of inverse participation ratio (IPR) for the gapless phase with  $\mu = 1$  corresponding to Fig. 4(a). (a) System without disorder. (b) System with chiral-symmetry-preserving disorder  $R = 0.1$ . The size of the system is  $M \times N = 60 \times 60$ .

right or left of the SSH chain. The condition  $|\delta_{k_y}| = |\mu + e^{ik_y}| < 1$  leads to  $\mu(\mu + 2 \cos k_y) < 0$ , and the interval of edge modes for  $k_y$  is

$$k_y \in \mathcal{I} = \begin{cases} (-\pi, -k_y^c) \cup (k_y^c, \pi], & 0 < \mu < 2 \\ (-k_y^c, k_y^c), & -2 < \mu < 0 \end{cases}. \quad (22)$$

with  $k_y^c = \arccos(-\mu/2)$ . The above interval  $\mathcal{I}$  matches with the interval with nonzero winding number in Eq. (20). The zero modes in the plot of energy band in Fig. 3(c3) and Fig. 3(e3) correspond this flat band of edge modes. For an arbitrary site-state  $a_{N,j}^\dagger |\text{vac}\rangle$  (or  $b_{1,j}^\dagger |\text{vac}\rangle$ ) at the edge, the total probability of on the component of edge state  $|\psi_R\rangle$  (or  $|\psi_L\rangle$ ) is

$$p = \frac{1}{N} \sum_{k_y \in \mathcal{I}} (1 - |\delta_{k_y}|^2) \approx \frac{1}{2\pi} \int_{\mathcal{I}} (1 - |\delta_{k_y}|^2) dk_y, \quad (23)$$

which is only  $\mu$  dependent in large  $N$  limit. We will see that  $p$  can be measured by LE of the edge site-state.

#### IV. DYNAMIC DETECTION OF EDGE MODES

In this section, we focus on the dynamics of the system in the presence of disorder. As we know, one of the most

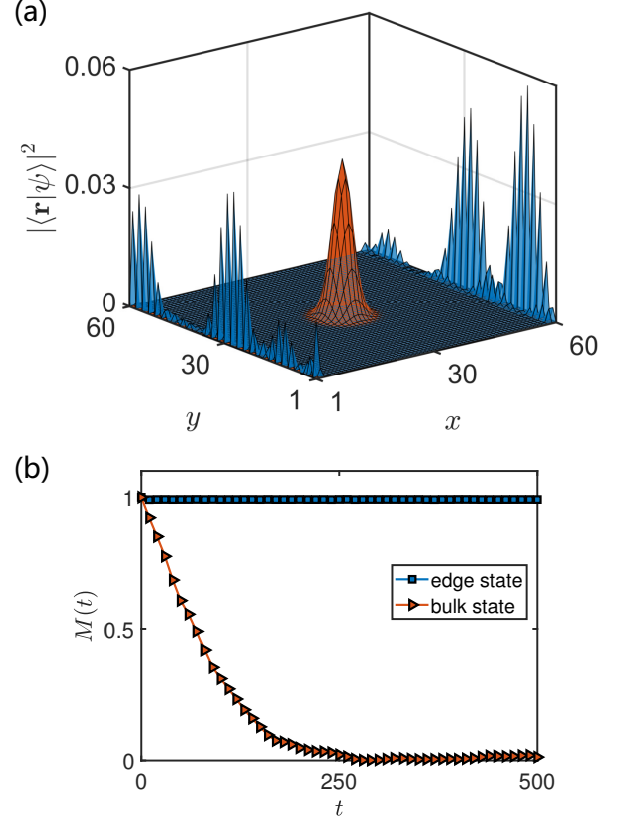


FIG. 6. (a) Profiles of initial states of numerical simulations for the LEs. The edge state (blue) is taken as the eigenstate of the system in cylindrical boundary condition without disorder and the bulk state (orange) is taken as the 2D Gaussian wavepacket. (b) Plots of numerical simulations for LEs as the functions of time. The initial states are taken as the edge state and bulk state shown in (a). It can be seen that LEs have diametrically opposite behaviors for the initial bulk and edge states. The time  $t$  is in units of  $J^{-1}$ , where  $J$  is the scale of the Hamiltonian and we take  $J = 1$ . The size of the system is  $M \times N = 60 \times 60$  and the disorder strength is  $R = 0.1$ .

striking features of topologically protected edge states is the robustness against to certain types of disordered perturbation to the original Hamiltonian. The disorder we discuss here arises from the hopping integrals in the Hamiltonian  $H$  from Eq. (4) with cylindrical boundary condition. In the presence of disorder, the Hamiltonian reads

$$H_D = \sum_{\mathbf{r}} (\mu_{\mathbf{r}} a_{\mathbf{r}}^\dagger b_{\mathbf{r}} + \nu_{\mathbf{r}} a_{\mathbf{r}}^\dagger b_{\mathbf{r}+\hat{x}} + \lambda_{\mathbf{r}} a_{\mathbf{r}}^\dagger b_{\mathbf{r}+\hat{y}}) + \text{h.c.}, \quad (24)$$

where parameters  $\{\mu_{\mathbf{r}}, \nu_{\mathbf{r}}, \lambda_{\mathbf{r}}\}$  are three set of position-dependent numbers. Here we take

$$\begin{cases} \mu_{\mathbf{r}} = \mu + d_{\mu,\mathbf{r}} \\ \nu_{\mathbf{r}} = 1 + d_{\nu,\mathbf{r}} \\ \lambda_{\mathbf{r}} = 1 + d_{\lambda,\mathbf{r}} \end{cases}, \quad (25)$$

where  $d_{\mu,\mathbf{r}}$ ,  $d_{\nu,\mathbf{r}}$ , and  $d_{\lambda,\mathbf{r}}$  are uniform random real numbers within the interval  $[-R, R]$ , taking the role of the

disorder strength, and  $\mathbf{r}$  is the site index.

Now we investigate the influence of nonzero  $R$  by comparing two sets of eigenvalues obtained by numerical diagonalization of finite-dimensional matrices of  $H$  and  $H_D$  in single-particle subspace, respectively. The plots in Fig. 4 indicate that the zero modes remain unchanged in the presence of chiral-symmetry-preserving random perturbations with not too large  $R$ . The chiral symmetry here is responsible for the existence of zero modes, in other words, under chiral-symmetry-breaking disordered perturbation, the zero modes no longer survive. Taking the disordered on-site potential for example, the Hamiltonian reads  $H' = H + \sum_{\mathbf{r}} (d_{a,\mathbf{r}} a_{\mathbf{r}}^\dagger a_{\mathbf{r}} + d_{b,\mathbf{r}} b_{\mathbf{r}}^\dagger b_{\mathbf{r}})$ , where  $d_{a,\mathbf{r}}$  and  $d_{b,\mathbf{r}}$  are uniform random real numbers within the interval  $[-R, R]$ . The numerical results in Fig. 4 indicate that under this kind of chiral-symmetry-breaking disordered perturbation, the zero modes do not survive, which may lead to the decay of the LE in contrast to Eqs. (2) and (3) though the original edge states remain localized in the edge. Furthermore, we investigate the inverse participation ratio (IPR) for the gapless phase with and without chiral-symmetry-preserving disorder. The IPR is defined as  $\text{IPR}(E) = \sum_{\mathbf{r}} |\langle \mathbf{r} | \psi_E \rangle|^4$ , with  $E$  denoting the energy levels and  $\mathbf{r}$  denoting the lattice sites. The numerical results of IPR shown in Fig. 5 indicate that all the states with energy  $E \neq 0$  are extended in the presence or absence of weak disorder, and the system is gapless in the transport sense.

According to the analysis in section II, the LEs should have diametrically opposite behaviors for the initial bulk and edge states, respectively. To verify this point, we compute the LEs for two initial states: (i) a Gaussian wave packet in the bulk  $|\psi_G\rangle$ ; (ii) an edge state  $|\psi_R\rangle$  or  $|\psi_L\rangle$ . In Fig. 6, we plot the result, which is in agreement with our prediction. We find that when  $|\psi(0)\rangle$  is a bulk state  $M(t)$  will decay exponentially, while  $M(t)$  keeps at the constant 1 when  $|\psi(0)\rangle = |\psi_R\rangle$  or  $|\psi_L\rangle$ . Accordingly,

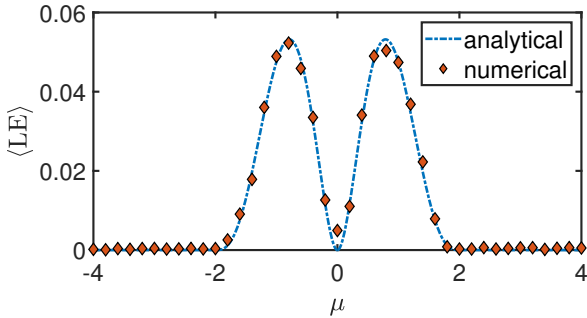


FIG. 7. Comparison of the average convergent LEs and analytical expression from Eq.(28) as the functions of  $\mu$ . The initial state is an edge site-state and the final time is  $t = 1000J^{-1}$ , where  $J$  is the scale of the Hamiltonian and we take  $J = 1$ . The size of the system is  $M \times N = 60 \times 60$  and the disorder strength is  $R = 0.1$ . It is found that the two results are in agreement with each other well. This means that the measurement of LE can identify the phase diagram.

when we take the initial state as the superposition of scattering and bound states, i.e.,

$$|\psi(0)\rangle = c_G |\psi_G\rangle + c_R |\psi_R\rangle + c_L |\psi_L\rangle, \quad (26)$$

with  $|c_G|^2 + |c_R|^2 + |c_L|^2 = 1$ , we can have the LE after long time

$$\lim_{t \rightarrow \infty} M(t) = |c_R|^2 + |c_L|^2 = 1 - |c_G|^2. \quad (27)$$

It indicates that the magnitude of  $c_G$  can be measured by the LE. Furthermore, if we take  $|\psi(0)\rangle = a_{N,j}^\dagger |\text{vac}\rangle$  (or  $b_{1,j}^\dagger |\text{vac}\rangle$ ), the population of survival zero modes is a function of  $\mu$ , which also relates to the quantity  $p$ , i.e.,

$$\lim_{t \rightarrow \infty} M(t) = \lim_{t \rightarrow \infty} |\langle \psi(0) | e^{iH_D t} e^{-iH_0 t} | \psi(0) \rangle|^2 \approx p^2, \quad (28)$$

for very weak disordered system  $H_D$ . It is presumably that the size of flat band  $k_c$  can be obtained by the LE in the dynamical process.

To demonstrate and verify this scheme, we perform numerical simulations. We choose three different strengths of chiral-symmetry-preserving disorder  $R$  and six typical values of hopping amplitudes  $\mu$ . The numerical simulations are performed ten times for each set of parameter. Fig. 3(a4-f4) plot the convergent LEs, where  $\text{LE} = \lim_{t \rightarrow \infty} M(t)$  is obtained by taking a sufficiently large  $t$  ( $t = 3000$ ), for several typical  $\mu$  with different strengths of chiral-symmetry-preserving disorder  $R = 0.04, 0.1$  and  $0.15$ . It indicates that a single measurement result depends on the setting random number. The average of multi-measurement result  $\langle \text{LE} \rangle$  is very close to the analytical result in the blue dashed lines. The dependence of  $\langle \text{LE} \rangle$  on  $\mu$  for a wide range of  $\mu$  with the disorder strength  $R = 0.1$  are presented in Fig. 7. The comparison between analytical and numerical results shows that the LE method has a good accuracy to determine the positions of vortices, as well as the phase diagram. The transition points occur at  $\mu = \pm 2$ , associated with the vanishing  $\langle \text{LE} \rangle$ .

The data and codes of the numerical calculations of Figs. 3-7 are available in supplementary material as well as in Zenodo<sup>58</sup>.

## V. DISCUSSION

In this work, we have proposed a way to detect the positions of two vortices in 2D momentum space, as well as the phase diagram. The advantage of this scheme is not limited by the imperfection of the system, but in the aid of the disorder. Photonic systems are a candidate for the realization of the scheme in experiment, beyond the solid-state electron systems. The field of topological photonics grows rapidly and aims to explore the physics of topological phases of matter in the context of optics. Photonic systems provide a natural and convenient medium to investigate fundamental quantum transport properties.

Using photons, one can selectively excite a site-state, and observe the spatial responses throughout the material, which are challenging tasks in electronic systems. Recently, it has been shown that Loschmidt echo of photons can be observed in a binary waveguide, by exchanging the two sublattices after some propagation distance<sup>59</sup>. The dynamic feature of topological edge states and phase diagram presented in this work potentially can be utilized for

developing inherently robust artificial photonic devices.

## ACKNOWLEDGMENT

This work was supported by National Natural Science Foundation of China (under Grant No. 11874225).

- 
- \* songtc@nankai.edu.cn
- <sup>1</sup> M. Z. Hasan and C. L. Kane, *Colloquium: Topological insulators*, Rev. Mod. Phys. **82**, 3045-3067 (2010).
  - <sup>2</sup> X. L. Qi and S. C. Zhang, *Topological insulators and superconductors*, Rev. Mod. Phys. **83**, 1057-1110 (2011).
  - <sup>3</sup> C. K. Chiu, J. C. Y. Teo, A. P. Schnyder and S. Ryu, *Classification of topological quantum matter with symmetries*, Rev. Mod. Phys. **88**, 035005 (2016).
  - <sup>4</sup> H. Weng, R. Yu, X. Hu, X. Dai and Z. Fang, *Quantum anomalous Hall effect and related topological electronic states*, Adv. Phys. **64**, 227-282 (2015).
  - <sup>5</sup> L. Fu and C. L. Kane, *Superconducting Proximity Effect and Majorana Fermions at the Surface of a Topological Insulator*, Phys. Rev. Lett. **100**, 096407 (2008).
  - <sup>6</sup> R. M. Lutchyn, J. D. Sau, and S. Das. Sarma, *Majorana Fermions and a Topological Phase Transition in Semiconductor-Superconductor Heterostructures*, Phys. Rev. Lett. **105**, 077001 (2010).
  - <sup>7</sup> V. Mourik, K. Zuo, S. M. Frolov, S. R. Plissard, E. P. A. M. Bakkers and L. P. Kouwenhoven, *Signatures of Majorana Fermions in Hybrid Superconductor-Semiconductor Nanowire Devices*, Science **336**, 1003 (2012).
  - <sup>8</sup> S. Nadj-Perge, I. K. Drozdov, J. Li, H. Chen, S. Jeon, J. Seo, A. H. MacDonald, B. A. Bernevig and A. Yazdani, *Observation of Majorana fermions in ferromagnetic atomic chains on a superconductor*, Science **346**, 602 (2014).
  - <sup>9</sup> Y. Oreg, G. Refael, and F. von Oppen, *Helical Liquids and Majorana Bound States in Quantum Wires*, Phys. Rev. Lett. **105**, 177002 (2010).
  - <sup>10</sup> N. Read and D. Green, *Paired states of fermions in two dimensions with breaking of parity and time-reversal symmetries and the fractional quantum Hall effect*, Phys. Rev. B **61**, 10267 (2000).
  - <sup>11</sup> A. H. C. Neto, F. Guinea, N. M. R. Peres, K. S. Novoselov and A. K. Geim, *The electronic properties of graphene*, Rev. Mod. Phys. **81**, 109 (2009).
  - <sup>12</sup> Z. K. Liu, J. Jiang, B. Zhou, Z. J. Wang, Y. Zhang, H. M. Weng, D. Prabhakaran, S.-K. Mo, H. Peng, P. Dudin, T. Kim, M. Hoesch, Z. Fang, X. Dai, Z. X. Shen, D. L. Feng, Z. Hussain and Y. L. Chen, *A stable three-dimensional topological Dirac semimetal Cd<sub>3</sub>As<sub>2</sub>*, Nat. Mater. **13**, 677-681 (2014).
  - <sup>13</sup> Z. K. Liu, B. Zhou, Y. Zhang, Z. J. Wang, H. M. Weng, D. Prabhakaran, S.-K. Mo, Z. X. Shen, Z. Fang, X. Dai, Z. Hussain and Y. L. Chen, *Discovery of a Three-Dimensional Topological Dirac Semimetal, Na<sub>3</sub>Bi*, Science **343**, 864 (2014).
  - <sup>14</sup> J. A. Steinberg, S. M. Young, S. Zaheer, C. L. Kane, E. J. Mele, and A. M. Rappe, *Bulk Dirac Points in Distorted Spinels*, Phys. Rev. Lett. **112**, 036403 (2014).
  - <sup>15</sup> Z. Wang, Y. Sun, X.-Q. Chen, C. Franchini, G. Xu, H. Weng, X. Dai, and Z. Fang, *Dirac semimetal and topological phase transitions in A<sub>3</sub>Bi (A=Na, K, Rb)*, Phys. Rev. B **85**, 195320 (2012).
  - <sup>16</sup> J. Xiong, S. K. Kushwaha, T. Liang, J. W. Krizan, M. Hirschberger, W. Wang, R. J. Cava and N. P. Ong, *Evidence for the chiral anomaly in the dirac semimetal Na<sub>3</sub>Bi*, Science **350**, 413-416 (2015).
  - <sup>17</sup> S. M. Young, S. Zaheer, J. C. Y. Teo, C. L. Kane, E. J. Mele, and A. M. Rappe, *Dirac Semimetal in Three Dimensions*, Phys. Rev. Lett. **108**, 140405 (2012).
  - <sup>18</sup> M. Hirschberger, S. Kushwaha, Z. Wang, Q. Gibson, S. Liang, C. A. Belvin, B. A. Bernevig, R. J. Cava and N. P. Ong, *The chiral anomaly and thermopower of Weyl fermions in the half-Heusler GdPtBi*, Nat. Mater. **15**, 1161-1165 (2016).
  - <sup>19</sup> S.-M. Huang, S.-Y. Xu, I. Belopolski, C.-C. Lee, G. Chang, B. Wang, N. Alidoust, G. Bian, M. Neupane, C. Zhang, S. Jia, A. Bansil, H. Lin and M. Z. Hasan, *A Weyl Fermion semimetal with surface Fermi arcs in the transition metal monophosphide TaAs class*, Nat. Commun. **6**, 7373 (2015).
  - <sup>20</sup> B. Q. Lv, H. M. Weng, B. B. Fu, X. P. Wang, H. Miao, J. Ma, P. Richard, X. C. Huang, L. X. Zhao, G. F. Chen, Z. Fang, X. Dai, T. Qian, and H. Ding, *Experimental Discovery of Weyl Semimetal TaAs*, Phys. Rev. X **5**, 031013 (2015).
  - <sup>21</sup> B. Q. Lv, N. Xu, H. M. Weng, J. Z. Ma, P. Richard, X. C. Huang, L. X. Zhao, G. F. Chen, C. E. Matt, F. Bisti, V. N. Strocov, J. Mesot, Z. Fang, X. Dai, T. Qian, M. Shi and H. Ding, *Observation of Weyl nodes in TaAs*, Nat. Phys. **11**, 724-727 (2015).
  - <sup>22</sup> C. Shekhar, A. K. Nayak, S. Singh, N. Kumar, S.-C. Wu, Y. Zhang, A. C. Komarek, E. Kampert, Y. Skourski, J. Wosnitzer, W. Schnelle, A. McCollam, U. Zeitler, J. Kubler, S. S. P. Parkin, B. Yan and C. Felser, *Observation of chiral magneto-transport in RPtBi topological Heusler compounds*, arXiv:1604.01641.
  - <sup>23</sup> X. Wan, A. M. Turner, A. Vishwanath and S. Y. Savrasov, *Topological semimetal and Fermi-arc surface states in the electronic structure of pyrochlore iridates*, Phys. Rev. B **83**, 205101 (2011).
  - <sup>24</sup> H. Weng, C. Fang, Z. Fang, B. A. Bernevig and X. Dai, *Weyl Semimetal Phase in Noncentrosymmetric Transition-Metal Monophosphides*, Phys. Rev. X **5**, 011029 (2015).
  - <sup>25</sup> S.-Y. Xu, N. Alidoust, I. Belopolski, Z. Yuan, G. Bian, T.-R. Chang, H. Zheng, V. N. Strocov, D. S. Sanchez, G. Chang, C. Zhang, D. Mou, Y. Wu, L. Huang, C.-C. Lee, S.-M. Huang, B. Wang, A. Bansil, H.-T. Jeng, T. Neupert, A. Kaminski, H. Lin, S. Jia, and M. Z. Hasan, *Discovery of a Weyl fermion state with Fermi arcs in niobium arsenide*, Nat. Phys. **11**, 748-754 (2015).



- <sup>26</sup> S.-Y. Xu, I. Belopolski, N. Alidoust, M. Neupane, G. Bian, C. Zhang, R. Sankar, G. Chang, Z. Yuan, C.-C. Lee, S.-M. Huang, H. Zheng, J. Ma, D. S. Sanchez, B. Wang, A. Bansil, F. Chou, P. P. Shibayev, H. Lin, S. Jia, and M. Z. Hasan, Discovery of a Weyl fermion semimetal and topological Fermi arcs, *Science* **349**, 613-617 (2015).
- <sup>27</sup> M. Fujita, K. Wakabayashi, K. Nakada and K. Kusakabe, Peculiar Localized State at Zigzag Graphite Edge, *J. Phys. Soc. Jpn.* **65**, 1920 (1996)
- <sup>28</sup> S. Ryu and Y. Hatsugai, Topological Origin of Zero-Energy Edge States in Particle-Hole Symmetric Systems, *Phys. Rev. Lett.* **89**, 077002 (2002)
- <sup>29</sup> W. Yao, S. A. Yang and Q. Niu, Edge States in Graphene: From Gapped Flat-Band to Gapless Chiral Modes, *Phys. Rev. Lett.* **102**, 096801 (2009)
- <sup>30</sup> K. Wakabayashi, Y. Takane and M. Sigrist, Perfectly Conducting Channel and Universality Crossover in Disordered Graphene Nanoribbons, *Phys. Rev. Lett.* **99**, 036601 (2007)
- <sup>31</sup> Z. B. Yan, R. Bi, and Z. Wang, Majorana Zero Modes Protected by a Hopf Invariant in Topologically Trivial Superconductors, *Phys. Rev. Lett.* **118**, 147003 (2017).
- <sup>32</sup> Z. B. Yan, F. Song, and Z. Wang, Majorana Corner Modes in a High-Temperature Platform, *Phys. Rev. Lett.* **121**, 096803 (2018).
- <sup>33</sup> Q. Y. Wang, C. C. Liu, Y. M. Lu and F. Zhang, High-Temperature Majorana Corner States, *Phys. Rev. Lett.* **121**, 186801 (2018).
- <sup>34</sup> T. Ozawa, H. M. Price, A. Amo, N. Goldman, M. Hafezi, L. Lu, M. C. Rechtsman, D. Schuster, J. Simon, O. Zilberberg and I. Carusotto, Topological photonics, *Rev. Mod. Phys.* **91**, 015006 (2019).
- <sup>35</sup> L. Lu, J. D. Joannopoulos, and M. Soljačić, Topological photonics, *Nat. Photonics* **8**, 821 (2014).
- <sup>36</sup> P. W. Anderson, Absence of Diffusion in Certain Random Lattices. *Phys. Rev.* **109**, 1492 (1958).
- <sup>37</sup> A. A. Chabanov, M. Stoytchev and A. Z. Genack, Statistical signatures of photon localization, *Nature* **404**, 850-853 (2000).
- <sup>38</sup> T. Schwartz, G. Bartal, S. Fishman and M. Segev, Transport and Anderson localization in disordered two-dimensional photonic lattices, *Nature* **446**, 52-55 (2007).
- <sup>39</sup> H. Hu, A. Strybulevych, J. H. Page, S. E. Skipetrov and B. A. van Tiggelen, Localization of ultrasound in a three-dimensional elastic network, *Nature Phys.* **4**, 945-948 (2008).
- <sup>40</sup> A. P. Schnyder and S. Ryu, Topological phases and surface flat bands in superconductors without inversion symmetry, *Phys. Rev. B* **84**, 060504(R) (2011).
- <sup>41</sup> A. P. Schnyder, P. M. R. Brydon, and C. Timm, Types of topological surface states in nodal noncentrosymmetric superconductors, *Phys. Rev. B* **85**, 024522 (2012).
- <sup>42</sup> K. L. Zhang, P. Wang and Z. Song, Majorana flat band edge modes of topological gapless phase in 2D Kitaev square lattice, *Sci. Rep.* **9**, 4978 (2019).
- <sup>43</sup> P. Wang, S. Lin, G. Zhang, and Z. Song, Topological gapless phase in Kitaev model on square lattice, *Sci. Rep.* **7**, 17179 (2017).
- <sup>44</sup> V. M. Pereira, A. H. C. Neto, and N. M. R. Peres, Tight-binding approach to uniaxial strain in graphene, *Phys. Rev. B* **80**, 045401 (2009).
- <sup>45</sup> H. Rostami, and R. Asgari, Electronic ground-state properties of strained graphene, *Phys. Rev. B* **86**, 155435 (2012).
- <sup>46</sup> H. H. Pu, S. H. Rhim, C. J. Hirschmugl, M. Gajdardziska-Josifovska, M. Weinert, and J. H. Chen, Strain-induced band-gap engineering of graphene monoxide and its effect on graphene, *Phys. Rev. B* **87**, 085417 (2013).
- <sup>47</sup> A. Sharma, V. N. Kotov, and A. H. C. Neto, Effect of uniaxial strain on ferromagnetic instability and formation of localized magnetic states on adatoms in graphene, *Phys. Rev. B* **87**, 155431 (2013).
- <sup>48</sup> D. A. Bahamon, and V. M. Pereira, Conductance across strain junctions in graphene nanoribbons, *Phys. Rev. B* **88**, 195416 (2013).
- <sup>49</sup> C.-K. Chiu, and A. P. Schnyder, Classification of reflection-symmetry-protected topological semimetals and nodal superconductors, *Phys. Rev. B* **90**, 205136 (2014).
- <sup>50</sup> F. D. M. Haldane, Berry Curvature on the Fermi Surface: Anomalous Hall Effect as a Topological Fermi-Liquid Property, *Phys. Rev. Lett.* **93**, 206602 (2004).
- <sup>51</sup> K. Sun, W. V. Liu, A. Hemmerich and S. D. Sarma, Topological semimetal in a fermionic optical lattice, *Nat. Phys.* **8**, 67-70 (2012).
- <sup>52</sup> E. I. Blount, Solid State Physics, Eds. F. Seitz and D. Turnbull, Vol. 13 (Academic, New York, 1962).
- <sup>53</sup> S. Matsuura, P.-Y. Chang, A. P. Schnyder, and S. Ryu, Protected boundary states in gapless topological phases, *New J. Phys.* **15**, 065001 (2013).
- <sup>54</sup> C. L. M. Wong, J. Liu, K. T. Law, and P. A. Lee, Majorana flat bands and unidirectional Majorana edge states in gapless topological superconductors, *Phys. Rev. B* **88**, 060504(R) (2013).
- <sup>55</sup> M. Milićević, T. Ozawa, G. Montambaux, I. Carusotto, E. Galopin, A. Lemaître, L. Le Gratiet, I. Sagnes, J. Bloch, and A. Amo, Orbital Edge States in a Photonic Honeycomb Lattice, *Phys. Rev. Lett.* **118**, 107403 (2017).
- <sup>56</sup> J. K. Asbóth, L. Oroszlány, and A. Pályi, A Short Course on Topological Insulators: Band Structure and Edge States in One and Two Dimensions, *Lecture Notes in Physics* (Springer International Publishing, Switzerland, 2016).
- <sup>57</sup> P. Delplace, D. Ullmo, and G. Montambaux, Zak phase and the existence of edge states in graphene, *Phys. Rev. B* **84**, 195452 (2011).
- <sup>58</sup> See online supplementary material, or Zenodo: <http://doi.org/10.5281/zenodo.3403408>
- <sup>59</sup> S. Longhi, Photonic Loschmidt echo in binary waveguide lattices, *Opt. Lett.* **42**, 2551 (2017).